Thresholds of secondary organic aerosol formation by ozonolysis of monoterpenes measured in a laminar flow aerosol reactor

6 AUTHORS, INCLUDING:

François Bernard
National Oceanic and Atmospheric Ad…
16 PUBLICATIONS **94** CITATIONS

Ivan Fedioun
CNRS Orleans Campus
23 PUBLICATIONS **95** CITATIONS

Thresholds of secondary organic aerosol formation by ozonolysis of monoterpenes measured in a laminar flow aerosol reactor

François Bernard, Ivan Fedioun, Fabrice Peyroux, Alain Quilgars, Véronique Daële, Abdelwahid Mellouki *

Institut de Combustion, Aérothermique, Réactivité et Environnement, Centre National de la Recherche Scientifique (ICARE-CNRS), 1C, Avenue de la Recherche Scientifique, 45071 Orléans cedex 02, France

ABSTRACT

The reactions of ozone with a series of monoterpenes (α-pinene, sabinene, limonene and myrcene) were investigated in a novel flow reactor dedicated to the investigation of secondary organic aerosol (SOA) formation. Rate constants for the gas phase reactions and nucleation thresholds were determined at $T \sim 296$ K, $P \sim 764$ Torr under dry conditions (dew point $\leq -33\ ^{\circ}$C) and in absence of OH radicals scavenger and seed particles. Comparison with the literature as well as data from a simulation chamber showed good agreement. The experiments also show that the novel flow reactor improves the accuracy in evaluating the nucleation thresholds during the ozonolysis of monoterpenes and show that aerosol flow reactor is a useful tool to study the SOA nucleation step. Given as an upper limit, the nucleation thresholds obtained are (in molecule cm^{-3}/ppb): α-pinene, 3.9×10^{10}/1.56; sabinene, 6.2×10^{9}/0.26; limonene, 1.1×10^{10}/0.43 and myrcene 2.1×10^{10}/0.83.

1. Introduction

Terrestrial vegetation has the largest contribution to Volatile Organic Compounds (VOCs) burden in the atmosphere (Guenther et al., 1995), isoprene and monoterpenes being the dominant on a global scale. Once emitted, these VOCs undergo chemical oxidation through reactions with ozone, OH and NO$_3$ radicals to form secondary products impacting strongly the tropospheric chemical composition (Atkinson & Arey, 2003). Oxidation reactions may lead to the formation of compounds with low volatility, able to nucleate and/or partition onto the pre-existing particles or even form new particles (Seinfeld & Pandis, 1998). Over the past decade, numerous field campaigns have shown the occurrence of nucleation events at different locations all over the world (Kulmala et al., 2004a). Through these observations, different nucleation mechanisms have been proposed such as, ion-induced nucleation (Enghoff & Svensmark, 2008), homogeneous nucleation for iodine containing compounds (O'Dowd et al., 2002a; Burkholder et al., 2004) and organic compounds (Hoppel et al., 2001; Burkholder et al., 2007), heterogeneous nucleation involving organic vapours able to condense on pre-existing particles (O'Dowd et al., 2002b; Kulmala et al., 2004b) and binary H$_2$O/H$_2$SO$_4$ (Kulmala & Laaksonen, 1990) and ternary H$_2$O/H$_2$SO$_4$/NH$_3$ (Kulmala et al., 2000) nucleation.

Secondary organic aerosols (SOA) formation has been observed in the atmosphere in forest, rural and urban areas (Kavouras & Stephanou, 2002; Volkamer et al., 2006; Zhang et al., 2007; Slowik et al., 2010) and intensively studied in laboratory over the recent years. Specific investigations have been conducted in order to identify the VOC precursors of SOA and the influence of environmental parameters (temperature, relative humidity, light and the presence of other gases

---

* Corresponding author. Tel.: +33 238257612; fax: +33 238696004.
  E-mail address: mellouki@cnrs-orleans.fr (A. Mellouki).

and seed particles) on their SOA mass formation potential (Hoffmann et al., 1997; Griffin et al., 1999; Cocker et al., 2001a,b; Presto et al., 2005a,b; Kroll et al., 2006; Lee et al., 2006a,b; Pathak et al., 2007). However, these formation processes remain an unresolved issue and more information about chemical and physical properties of nucleation agents are still required (Kanakidou et al., 2005; Hallquist et al., 2009).

In particular, it has been shown that SOA are formed via nucleation of atmospheric organic vapours on pre-existing particles observed in various rural environments where the organic fraction represents the major part of the observed nano-particles (Kulmala et al., 2004a). Therefore, various laboratory studies have been performed to investigate the nucleation potential of different nucleation precursor reactions using mainly atmospheric simulation chamber under controlled conditions (i.e. temperature, pressure, composition of gas mixture, irradiation). However, from the beginning of the reaction, aerosols undergo condensation and coagulation limiting the observation time in the first steps of the oxidation processes. In this regard, the flow reactor is a useful tool to accurately observe nucleation processes. It allows studying SOA formation potential from the first steps of the reaction. One of the advantages of this device is to generate particles under continuous flow with similar physical and chemical properties under fixed and controlled conditions (initial concentrations, temperature, pressure and reaction time). The other advantage is the possibility to conduct investigations at low reaction time enabling to have access to the early stages of the reaction. Beyond the nucleation process studies, aerosol flow tube allows to obtain data on the aerosol mass yield under different conditions (temperature, relative humidity, in the presence of OH radical or/and Criegee scavengers) (Bonn & Moortgat, 2002, 2003; Jonsson et al., 2006, 2008a,b; von Hessberg et al., 2009). Although flow reactor studies permit an in-depth comprehension of SOA formation processes, only few studies have reported the SOA formation potential of new particles as function of the consumed concentration of relevant atmospheric species (Koch et al., 2000; Berndt et al., 2003; Lee & Kamens, 2005).

The aim of the present work was to evaluate the SOA formation potential (in terms of number) from the ozonolysis of four monoterpenes: α-pinene, sabinene, limonene and myrcene and at later stage, to obtain the nucleation thresholds. This study did not aim at reproducing the previous results but rather to determine if the formation potential of aerosols through the reaction the ozone (and OH radicals) is higher than expected and thus lowering the nucleation thresholds through the use of a suitable set-up. A newly developed laminar flow reactor was used to conduct this study. In order to validate the flow reactor experimental conditions, pseudo-first order kinetic studies have been performed and the derived results have been compared to those obtained using atmospheric simulation chamber and to literature data. Therefore, the rate constants of the reactions of ozone with α-pinene, sabinene, myrcene and limonene obtained in this work were further used to estimate the SOA number formation potentials. The results from this work are compared with those from the literature when available.

2. Experimental methods

2.1. Flow reactor

SOA formation studies have been performed under controlled conditions using an aerosol flow tube recently developed at ICARE-CNRS laboratory. The experimental set-up is a combination of a laminar aerosol flow tube and a condensation particle counter (Fig. 1). The reactor consists of a vertical 100 cm long with 10 cm i.d. made of Pyrex glass and a movable injector (110 cm length and 1.2 cm i.d.). Reaction time (or residence time, t) was varied by adjusting the position of the movable mixing plunger relatively to the sampling point at the bottom of the reactor. The organic compounds were diluted in N_2 (typically $\alpha \sim 0.05\%$) and stored in a Pyrex reservoir. Synthetic air and N_2 (the bath gases) passed through HEPA filters (TSI) in order to eliminate the particles which could be present in the gas cylinders. Ozone is generated through the photolysis of oxygen using a Hg Pen-ray lamp. Mixing ratio of ozone in the reactor is controlled by varying the ratio of synthetic air and N_2 flows. It is introduced into the flow reactor, separately from the monoterpenes, through the movable injector. Its concentration is measured at the outlet of the reactor by an ozone monitor based on UV absorption (model 49C, Thermo Environmental Instruments Inc or Horiba APOA-360). Experiments have been performed at $T \sim 296$ K, $P \sim 764$ Torr and with a dew point $\leq -33\,^{\circ}$C (relative humidity $\leq 1\%$). Relative humidity and temperature are continuously recorded at the outlet of the reactor using a combined probe (Vaisala HMT330 series transmitters). In addition, temperature is also measured inside the mixing plunger using a thermocouple.

In the reactor, the "ozone flow" (2.8 L min^{-1}) through the injector is composed of synthetic air and ozone diluted in N_2. The "external flow" (1.8 L min^{-1}) is a mixture of synthetic air/monoterpenes. Both flows are rapidly mixed under a turbulent regime, within less than 1 s, in a "mixing zone" positioned at the end of the movable injector. All flows are monitored with calibrated mass flow controllers (Celerity and Bronkhorst models). The pressure in the reactor is controlled by pressure transducer/controller and a regulation valve (Bronkhorst high-Tech, 5 L min^{-1}) enabling to adjust the outlet total flow in order to obtain the desired pressure in the reactor. Gas or aerosol samples are collected through an orifice centred at the bottom of the reactor with an inner diameter of 2.3 cm. In the configuration of this experimental set-up, the residence time from the sampling orifice to the instrument (condensation particle counter and ozone analyser) was estimated to be < 1 s. The outlet flow is pumped by a dry vacuum pump (Boc Edwards, XDS 10). All the parameters (P, T, ozone concentration and flows) are acquired using a computer equipped with National Instrument A/D Boards and can be viewed in real time using Labview software (Laview 7.1).
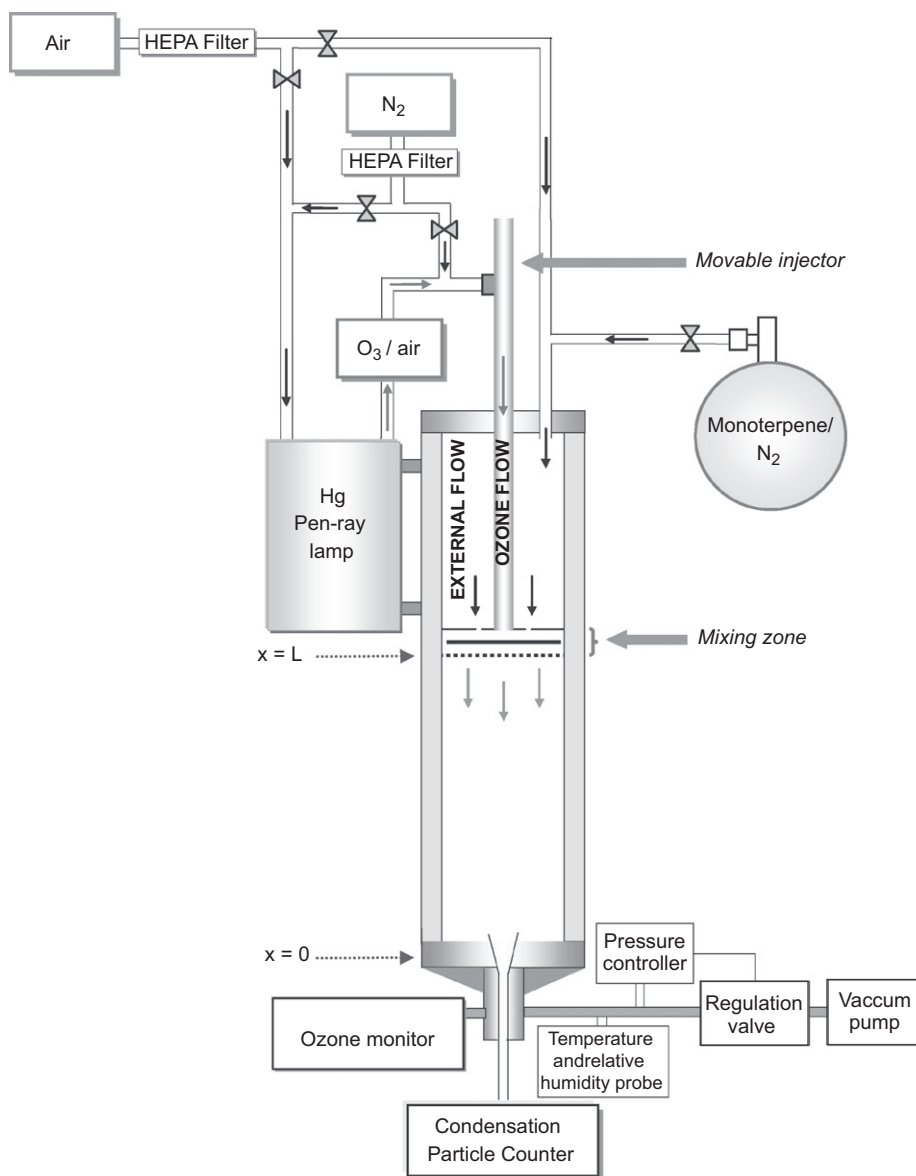
Fig. 1. Schematic of the flow tube reactor set-up configured for particle number measurement.

One of the most critical aspects of this type of experimental systems is the residence time in the reactor. In the study, it has been determined experimentally by nebulising a NaCl solution through the flow reactor using an atomizer (TSI Model 3076) with a reservoir containing an aqueous solution of sodium chloride (0.1 g cm^{-3}). Two condensation particle counters (CPC, TSI 3022A and TSI 3010) were used to measure the residence time. The first CPC was sampling from the entrance to the inlet of the mixing plunger while the second one was sampling from the outlet of the flow reactor. The residence time has been characterised for every 10 cm from 30 to 80 cm. Experiments have been repeated for different positions of the movable injector. The residence time results from the average of at least six measurements (the uncertainty is one-standard deviation on the average, 1σ). The distance between the movable inlet and the outlet of the reactor was varied and the residence time of NaCl particles in the flow tube versus the distance of the mixing zone to sampling point was recorded. The flow velocity, Ve$=(1.57 \pm 0.04)$ cm s^{-1}, was determined from the linear fit to the data (Fig. 2). Additional run was made by inversing the position of both CPCs in order to observe the influence of sampling flow on the measured residence time. In our experimental conditions, the total flow rate was 4.6 L min^{-1}. This leads to a Reynolds number $Re \sim 107$ ($\ll 2000$) and a Knudsen number of 6.6×10^{-7}, corresponding to a laminar and viscous flow.

These experimental derived values have been compared to numerical simulations using the FLUENT 6.3.26 software. The numerical procedure and the results are described hereafter. Fig. 3 shows the computational domain and the mesh for the 2D, axi-symmetric flow simulations. In the sampling region, the mesh is unstructured except near the solid walls
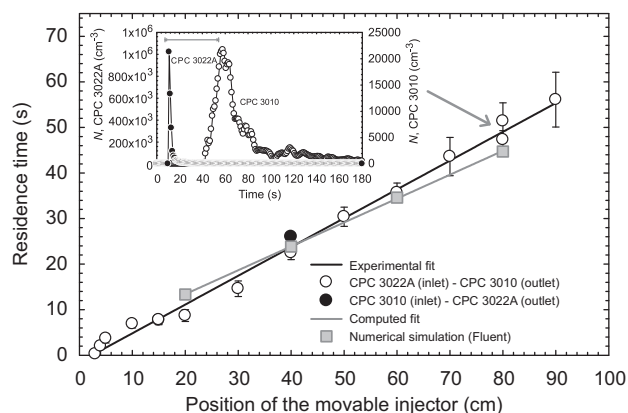
Fig. 2. Experimental and computed residence times of NaCl particles as function of the position of the movable mixing plunger in the flow reactor. The inserted graph shows an example of particle counting for one experiment for 80 cm length. Black dot represents one measurement at 40 cm where the position of CPCs Model 3022A and Model 3010 was inversed.
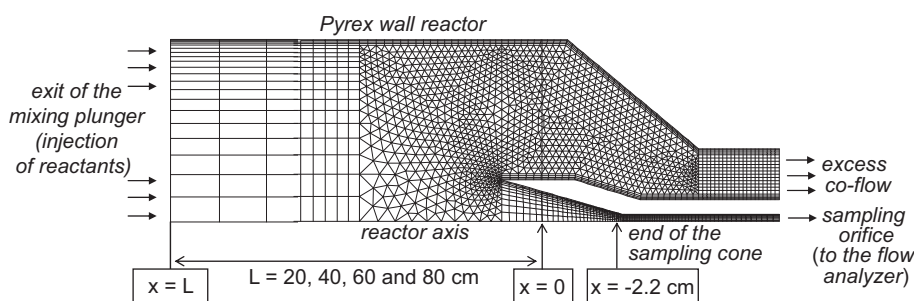

Fig. 3. Sketch of the mesh and the computational domain for the simulation of the flow reactor.

where rectangular cells are used to properly describe the boundary layer. In the reactor, the mesh is fully structured. Calculations have been made using the 2nd order upwind implicit pressure-based solver, and the SIMPLE algorithm for pressure–velocity coupling. The fluid is assumed to be air with constant properties (density, $\rho = 1.225$ kg m^{-3}; viscosity, $\mu = 1.7894 \times 10^{-5}$ kg m^{-1} s^{-1}). Boundary conditions are:

- no-slip on solid walls;
- imposed mass flow rate $Q_m = 9.392 \times 10^{-5}$ kg s^{-1} at the inlet at $x = L$ ($Q_v = 4.6$ L min^{-1});
- constant pressure $P_{co\text{-}flow} = P_{ref} = 760$ Torr at the excess co-flow outlet;
- constant pressure P_{sampl} at the sampling orifice.

The pressure difference $\Delta P = P_{co\text{-}flow} - P_{sampl}$ is adjusted to achieve the desired sampling mass flow rate. Simulations have been performed for four positions of the movable injector $L = 20$, 40, 60 and 80 cm, covering the working distance for the position of the mixing plunger, and for three different sampling flow rates $Q_{sampl} = 0.40$, 0.55 and 1.25 L min^{-1}. These flow rates have been chosen as representative from sampling flow of instruments which are usually connected at the outlet of the reactor: Scanning Mobility Particle Sizer (0.4 L min^{-1}), CPC Model 3010 (0.55 L min^{-1}) and CPC Model 3022A (1.25 L min^{-1}). The pressure differences obtained (in Torr) are 9.23×10^{-3}, 1.40×10^{-2} and 4.66×10^{-2} corresponding to the requested different flow rates 0.40, 0.55 and 1.25 L min^{-1}, respectively. The pressure difference values do not depend on the positions of the movable injector and the sampling flow rate does not influence significantly the inlet total pressure. In each case, convergence to residuals below 10^{-8} is obtained after about 450 iterations, and the mass balance accuracy is below 10^{-12} kg s^{-1}.

In the reactor, velocity profiles set-up about 3 diameters downstream from the inlet. They exhibit the parabolic shape of a laminar pipe flow. In order to compute the residence time of reactants, fluid particles are released numerically from cell centres at the inlet (20 cells), and are followed in a lagrangian description until they leave the computational domain, either captured by the sampling cone or ejected with the co-flow. Particles are numbered from #1 in the near-wall cell to #20 in the near-axis cell. Fig. 4 shows the flow streamlines, i.e. the particles trajectories in the case $L = 40$ cm, $Q_{sampl} = 0.55$ L min^{-1}. Three particles enter the sampling cone, #18, #19 and #20. In the case $Q_{sampl} = 0.40$ L min^{-1}, only two are captured (#19 and #20), and at the higher sampling mass flow rate $Q_{sampl} = 1.25$ L min^{-1}, five particles are captured from #16 to #20. The residence time of a particle is obtained from the hodograph $x(t)$, as the time at which the
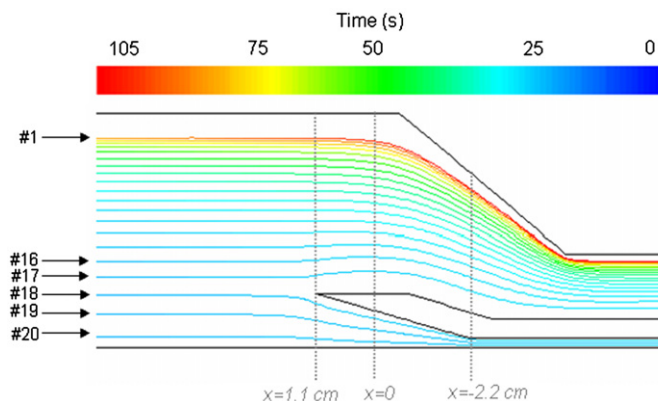
Fig. 4. Example of Lagrangian trajectories of numerical particles released from the inlet with $Q_{sampl} = 0.55 \, \text{L min}^{-1}$ where particles #18, #19 and #20 are captured by the sampling cone. For $Q_{sampl} = 1.25 \, \text{L min}^{-1}$, particles #16–#20 are captured by the sampling cone.
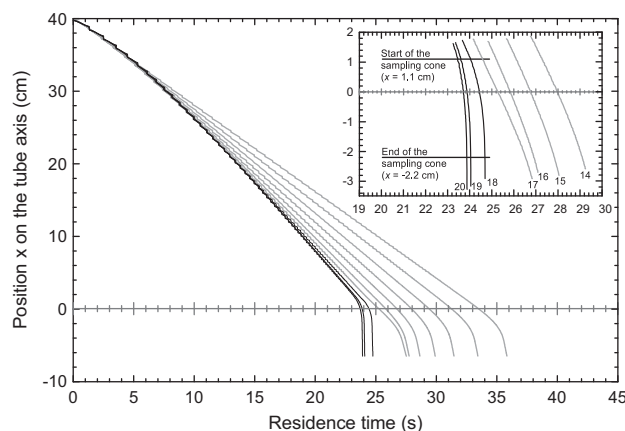

Fig. 5. Example of hodograph $x(t)$ of particles released from the inlet with $L=40$ cm and $Q_{sampl} = 0.55 \, \text{L min}^{-1}$.

particle crosses the line $x = -2.2$ cm which corresponds to the end of the sampling cone. Fig. 5 gives an illustration of the method. The residence time of particles should theoretically increase linearly with L, if the sampling flow rate is small compared to the overall flow rate. However, sampling flow rates are not negligible and induce an acceleration of the flow at the sampling cone inlet. Hence, for a given position L, the residence time decreases slightly with increasing the sampling flow rate, and the effect is more important for small L. Increasing the sampling flow rate from 0.4 to 1.25 L min^{-1} decreases the residence time of 1.5% (resp. 1.6%) for $L=80$ cm, and of 5.5% (resp. 5.8%) for $L=20$ cm, for particle #19 (resp. #20). They are almost the same for the two considered particles and vary linearly with the tube length. Fig. 2 compares these numerical data with the experimentally measured residence times and shows that the agreement is quite good with the average velocity recovered within 18% of accuracy.

During the SOA formation studies, experiments have been performed with a CPC Model 3022A in inlet high flow mode (1.25 L min^{-1}) leading to a diameter of the sampling flow estimated to 3.7 cm. According to numerical simulations, this implies that more particles are captured by the sampling cone. However, as shown in Fig. 2, changing the sampling flow at the outlet of the reactor agreed with numerical simulation and does not change the residence time obtained from a statistical point of view.

2.2. ICARE simulation chamber

The ICARE chamber has been described in detail elsewhere (Bernard et al., 2010), therefore, only a brief description is given here. Experiments were carried out in a 7300 L Teflon chamber in the dark at 303 ± 2 K and 760 Torr total pressure of dry purified air (< -29 °C of dew point). Rapid mixing of reactants was ensured within 1–2 min using a set of two fans made of Teflon fitted into the chamber. After each experiment, the chamber was flushed with purified air for at least 12 h. Reactants were introduced into the chamber via liquid phase by streaming purified air (gently heated when necessary). Temperature and relative humidity data were recorded by a combined sensor (T870-Series T800, Dostmann electronic). Reactants were monitored by *in situ* Fourier Transform Infra Red absorption spectroscopy (Nicolet 5700 Magna FT-IR spectrometer) coupled to a white-type mirror system resulting of an optical path of about 148 m.

3. Chemicals

The origin of the chemicals and their stated purity levels are: α-pinene (Sigma Aldrich, 98%), sabinene (Interchim, > 99%), limonene (Fluka, ≥ 98%), myrcene (Sigma Aldrich, 90%), cyclohexene (Fluka, 99%), cis-cyclooctene (Aldrich, 95%) and cyclohexane (Riedel-de Haën, 99.5%). For the flow tube experiments, chemicals were further purified by repeated cycle freeze in liquid nitrogen, pump and thaw cycles and fractional distillation before use.

4. Results and discussion

4.1. Kinetic measurements

The experiments have been conducted using both systems: flow reactor and simulation chamber. Initial conditions of experiments have been designed in accordance with the quantification limit of analytical instruments, leading to the expected rate constants with a good accuracy. One does not need to use ambient concentrations to determine reactions rate constants.

4.1.1. Flow reactor

Experiments were performed under pseudo-first order conditions where the organic reactant was introduced in higher excess compared to that of ozone. During the kinetics experiments, ozone concentration was measured at various reaction times by adjusting the position of the movable mixing plunger, in the presence and in the absence of the reactant. The decrease of ozone concentration can be expressed as $-\ln[O_3]_t = k'_{MEAS} \times t - \ln[O_3]_0$ where $[O_3]_t$ and $[O_3]_0$, represent the concentrations of ozone (in molecule cm^{-3}), at a reaction time t and the initial one, respectively, k'_{MEAS}, the pseudo-first order rate constant of the ozonolysis reaction with the studied monoterpene (in s^{-1}), and t, the reaction time (in second). For each concentration of monoterpene, $-\ln[O_3]_t = f(t)$ is constructed from which the pseudo-first order k'_{MEAS} rate constant is extracted by applying a least square analysis on the experimental data sets and corrected for radial diffusion (see below). The procedure is repeated for different concentrations of the compound. A plot of $k' = f([\text{monoterpenes}]_0)$ permits to obtain the bimolecular rate constant of the ozonolysis reaction, k. The quoted error on the rate constant was derived from the uncertainty on the slope corresponding to one-standard deviation (1σ).

The following initial conditions were used to derive the rate constants for the reactions of ozone with the four investigated monoterpenes: $[\text{monoterpene}]_0 = (2.1-29.7) \times 10^{13}$ molecule cm^{-3}; $[O_3]_0 = (1.4-5.5) \times 10^{12}$ molecule cm^{-3} and reaction time $t = 17-48$ s. Ozone loss on the wall of the reactor in absence of the organic compounds has been estimated before each kinetic run. In our experimental conditions where $[\text{monoterpene}]_0 \gg [O_3]_0$, the rate constants were derived from the loss of ozone. This latter may be subject to diffusion processes, its diffusion coefficient in air ($D_{O_3\text{-Air}}$) was estimated to be 0.164 cm^2 s^{-1} at 293 K (Massman, 1998). The plug-flow approximation where

$$\frac{k'_{MEAS} \times R^2}{D_{O_3\text{-Air}}} \leq 1.5 \tag{1}$$

with k'_{MEAS} is the measured pseudo-first order rate constant (in s^{-1}), R is the inner radius of the flow tube (in cm) and $D_{O_3\text{-Air}}$ is the diffusion coefficient of ozone in air (in cm^2 s^{-1}) can be applied to experimental system for $k'_{MEAS} \leq 9.84 \times 10^{-3}$ s^{-1} and the concentration of ozone is homogeneous all over the flow section. For $k'_{MEAS} > 9.84 \times 10^{-3}$ s^{-1}, the measured pseudo-first order rate constant has been corrected for radial diffusion using the formula: $k' = k'_{MEAS} \times (1 + D_{eff} \times k'_{MEAS}/Ve^2)$ with $D_{O_3\text{-Air,eff}} = D_{O_3\text{-Air}} + R^2 \times Ve^2/(48 \times D_{O_3\text{-Air}})$ where $D_{O_3\text{-Air,eff}}$ is the effective diffusion coefficient, preferred to $D_{O_3\text{-Air}}$ (Kaufman, 1984). The correction factor applied to k'_{MEAS} for the studied monoterpenes ranged from 1.03 to 1.14. Furthermore, the value of $k' \times D_{O_3\text{-Air}}/Ve^2$ (where k'_{MEAS}, $D_{O_3\text{-Air}}$ and Ve are defined above) is found to be $2.9 \times 10^{-3} \ll 1$ ($k'_{MEAS, max} = 4.4 \times 10^{-2}$ s^{-1}) which indicates that axial diffusion can be considered negligible in our conditions and therefore, k'_{MEAS} has not been corrected.

The pseudo-first order rate constant of ozone loss is $k_W(O_3) = (8 \pm 4) \times 10^{-4}$ s^{-1} in the absence of any organic reactant. In the presence of the organic compounds, k' has been measured to be $(0.4-5.0) \times 10^{-2}$ s^{-1}. $-\ln[O_3]_t = f(t)$ relationship was then applied to the experimental data sets for the series of the studied monoterpenes to derive the kinetic parameters. Fig. 6 displays an example of the ozone concentration at different reaction times in the presence of different concentrations of sabinene. Fig. 7 shows the plot of the pseudo-first order rate constant k' as function of sabinene concentration. Pseudo-first order fits for studied monoterpenes show a good linearity ($0.74 < r^2 < 0.96$). Bimolecular rate constants, k, were deduced from the least-square analysis on the experimental data and the quoted error corresponds to one-standard deviation on the slope (1σ). The use of large excess of monoterpenes over ozone ($[\text{Monoterpene}]_0/\Delta[O_3]$ ranged from 22 to 97) enables to make secondary ozone reactions such as with OH radicals and HO$_2$ negligible (O$_3$ reactions with OH and HO$_2$ not being extremely fast compared to that with monoterpenes ($k(O_3 + OH) = 7.3 \times 10^{-14}$ and $k(O_3 + HO_2) = 2.0 \times 10^{-15}$ cm^3 molecule^{-1} s^{-1}, (Atkinson et al., 2004))). Unsaturated intermediates (such as 4-methylenehex-5-enal and 3-isopropenyl-6-oxo-heptanal originating respectively from myrcene and limonene oxidations) could also react with ozone but will not affect the ozone concentrations in our conditions because of their low concentrations and low reaction rate constants compared to those with monoterpenes ($k_{4\text{-methylenehex-5-enal}} = (1.46 \pm 0.12) \times 10^{-17}$ cm^3 molecule^{-1} s^{-1} (Baker et al., 2004) and $k_{3\text{-isopropenyl-6-oxo-heptanal}} = (8.3 \pm 2.2) \times 10^{-18}$ cm^3 molecule^{-1} s^{-1} (Calogirou et al., 1999)).
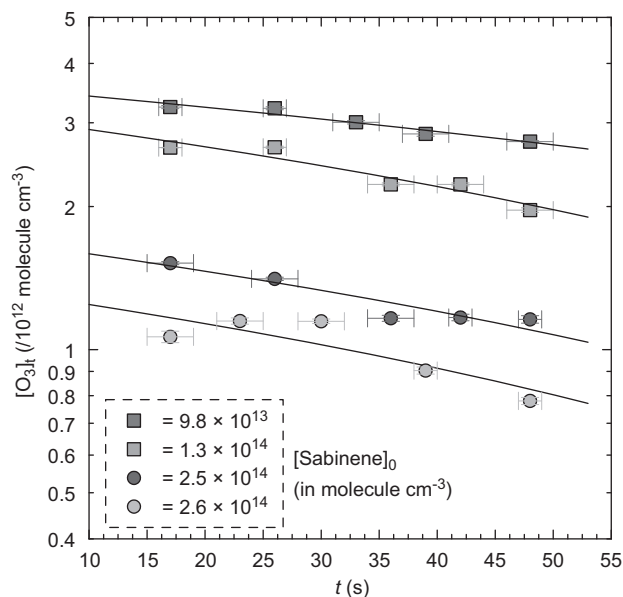
Fig. 6. Reaction of ozone with sabinene: example of pseudo-first order plots obtained at 297 ± 1 K.
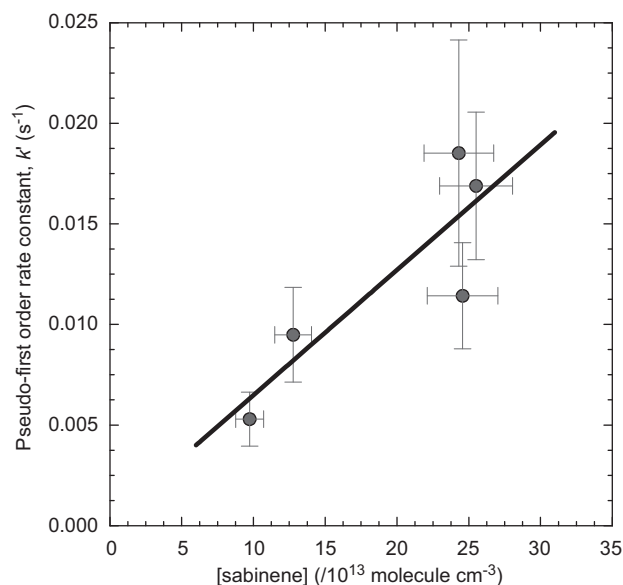
Fig. 7. Reaction of ozone with sabinene: pseudo-first order constant as function of concentration of sabinene from the ozonolysis reaction at 297 ± 1 K and 762 ± 3 Torr.

Experimental conditions and measured values of k' are listed in Table 1. The rate constants (in cm^3 molecule^{-1} s^{-1}) obtained for the investigated reactions at 297 ± 2 K and 765 ± 4 Torr are the following:

α-pinene$+O_3 \rightarrow$ Products $k = (1.1 \pm 0.1) \times 10^{-16}$
sabinene$+O_3 \rightarrow$ Products $k = (6.2 \pm 2.1) \times 10^{-17}$
limonene$+O_3 \rightarrow$ Products $k = (3.8 \pm 0.3) \times 10^{-16}$
myrcene$+O_3 \rightarrow$ Products $k = (5.7 \pm 1.6) \times 10^{-16}$
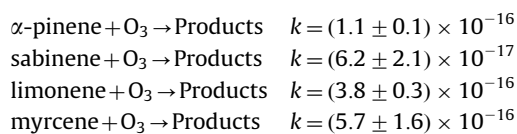
4.1.2. Simulation chamber experiments

Measurements of the rate constants were conducted using the well established relative rate method. Kinetic data were derived by monitoring the loss of monoterpenes relative to one reference compound. The references used in this

Table 1
Initial conditions and results obtained from the absolute measurements of rate constants for a series of monoterpenes by reaction with ozone at 297 ± 2 K and 765 ± 4 Torr.

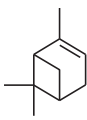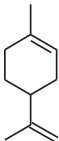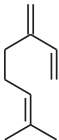| Monoterpenes	Structure	T (K)	[monoterpene]/10^{13} (molecule cm^{-3})	$(k' \pm 1\sigma)/10^{-2}$ (s^{-1})
α-Pinene		295	5.80	0.43 ± 0.13
		295	8.29	0.87 ± 0.12
		296	10.3	0.75 ± 0.26
		296	13.3	1.27 ± 0.07
		296	15.4	1.37 ± 0.20
		296	21.4	2.64 ± 0.24
		296	24.8	2.12 ± 0.18
		296	29.7	3.28 ± 0.17
			$k = (1.1 \pm 0.1) \times 10^{-16}$ cm^3 molecule^{-1} s^{-1}	
Sabinene		296	9.73	0.53 ± 0.13
		298	12.8	0.95 ± 0.24
		296	24.3	1.85 ± 0.56
		297	24.6	1.14 ± 0.26
		297	25.5	1.69 ± 0.37
			$k = (6.2 \pm 2.1) \times 10^{-17}$ cm^3 molecule^{-1} s^{-1}	
Limonene		296	2.10	0.65 ± 0.14
		298	3.28	0.85 ± 0.17
		296	3.31	1.15 ± 0.27
		297	4.04	1.31 ± 0.14
		297	5.00	1.81 ± 0.21
		299	6.35	1.78 ± 0.23
		297	6.99	2.53 ± 0.33
		297	10.1	3.73 ± 0.63
			$k = (3.8 \pm 0.3) \times 10^{-16}$ cm^3 molecule^{-1} s^{-1}	
Myrcene		298	2.68	1.33 ± 0.15
		297	3.58	1.15 ± 0.34
		298	4.46	2.82 ± 0.52
		296	6.45	2.30 ± 0.31
		298	8.68	4.97 ± 1.28
			$k = (5.7 \pm 1.6) \times 10^{-16}$ cm^3 molecule^{-1} s^{-1}	

study are *cis*-cyclooctene, $k_{O_3} = 3.86 \times 10^{-16}$ cm^3 molecule^{-1} s^{-1} (Cusick & Atkinson, 2005) and cyclohexene, $k_{O_3} = 8.1 \times 10^{-17}$ cm^3 molecule^{-1} s^{-1} (Calvert et al., 2000). These references are suitable for FT-IR analysis where a weak overlapping of IR bands is observed between the studied compounds and references. The loss rates of monoterpene and reference compounds in absence of ozone, k_L(monoterpene) and k_L(ref), (in s^{-1}), respectively, were measured before each run and the values obtained have been considered in the treatment of the data. Providing that the monoterpenes and the references were lost only by reaction with ozone and by dilution, and then it can be shown that

$$\ln\left(\frac{[\text{monoterpene}]_0}{[\text{monoterpene}]_t}\right) - k_L(\text{monoterpene}) \times t = \frac{k_{\text{monoterpene}}}{k_{\text{ref}}}\left(\ln\left(\frac{[\text{ref}]_0}{[\text{ref}]_t}\right) - k_L(\text{ref}) \times t\right) \qquad (2)$$

where [monoterpene]$_0$, [monoterpene]$_t$, [ref]$_0$ and [ref]$_t$ are the concentrations of the monoterpene and reference at times t_0 and t, and $k_{\text{monoterpene}}$ and k_{ref} are the rate constants for reactions of monoterpene and the reference with O$_3$. Plots of $(\ln([\text{monoterpene}]_0/[\text{monoterpene}]_t) - k_L(\text{monoterpene}) \times t)$ versus $(\ln([\text{ref}]_0/[\text{ref}]_t) - k_L(\text{ref}) \times t)$ pass through the origin and have a slope of $k_{\text{monoterpene}}/k_{\text{ref}}$. Reactants and reference compounds were monitored by FT-IR spectroscopy using absorption features over the following wavenumber ranges (cm^{-1}): α-pinene, 756–809; sabinene, 840–900; limonene 865–917/820–772; myrcene 870–930, *cis*-cyclooctene, 730–782 and cyclohexene, 1106–1172/841–952. The experiments were conducted in the presence of excess of cyclohexane to avoid secondary reactions with OH radicals which could be formed through the ozonolysis reactions (Paulson et al., 1999; Aschmann et al., 2002). The experiments have been repeated to enable us to derive averaged ratios for $k_{\text{monoterpene}}/k_{\text{Ref.}}$. One to two runs have been performed for the same initial conditions. The quoted uncertainties on the obtained rate constants originate from the uncertainties associated to the value of the slope (one-standard deviation, 1σ).

Initial concentrations (in molecule cm^{-3}) were: [monoterpenes]$_0$ = $(1.9 - 3.6) \times 10^{13}$, [references]$_0$ = $(1.8 - 5.2) \times 10^{13}$ and [cyclohexane]$_0 \sim 6.3 \times 10^{15}$. Preliminary checks consisted in observing temporal behaviour of monoterpenes and reference compound in the presence of an excess of cyclohexane for a duration of 45 min to 2 h which enables to determine their loss rates in absence of ozone. These loss rates were found to be in the range $(1.0 - 2.0) \times 10^{-5}$ s^{-1} for terpenes and $(1.0 - 1.8) \times 10^{-5}$ s^{-1} for the reference compounds. After addition of ozone to the gas mixtures, the loss of the reactants due to the ozonolysis was found to account for $\geq 96\%$ for terpenes and $\geq 97\%$ for the references. The durations of the runs in presence of all reactants were between 10 and 30 min depending on the reactivity of terpenes leading to a total consumption ranging from 14% to 99% for terpenes and reference compounds. Linear square analysis of the data gives the results shown in Table 2. The measured rate constants ratios

Table 2
Reaction of O_3 with the studied monoterpenes: summary of the experimental conditions and results from the relative rate study at 303 ± 2 K and 760 Torr of purified air (experiments were conducted in the presence of an excess of cyclohexane).

Monoterpenes	References	No. of runs	T (K)	($k/k_{ref} \pm 1\sigma$)	($k \pm 1\sigma$) (cm^3 molecule^{-1} s^{-1})
α-Pinene	Cyclohexene	2	302 ± 1	1.09 ± 0.10	$(8.8 \pm 0.8) \times 10^{-17}$
	Cis-cyclooctene	1	302 ± 1	0.27 ± 0.01	$(1.05 \pm 0.04) \times 10^{-16}$
				$k=(9.6 \pm 1.6) \times 10^{-17}$ cm^3 molecule^{-1} s^{-1}	
Sabinene	Cyclohexene	2	303 ± 1	1.05 ± 0.09	$(8.5 \pm 0.7) \times 10^{-17}$
	Cis-cyclooctene	2	303 ± 2	0.22 ± 0.03	$(8.3 \pm 1.2) \times 10^{-17}$
				$k=(8.4 \pm 1.3) \times 10^{-17}$ cm^3 molecule^{-1} s^{-1}	
Limonene	Cyclohexene	2	302 ± 1	2.3 ± 0.2	$(1.9 \pm 0.2) \times 10^{-16}$
	Cis-cyclooctene	2	303 ± 1	0.55 ± 0.08	$(2.1 \pm 0.3) \times 10^{-16}$
				$k=(2.0 \pm 0.4) \times 10^{-16}$ cm^3 molecule^{-1} s^{-1}	
Myrcene	Cyclohexene	2	303 ± 1	5.7 ± 0.8	$(4.6 \pm 0.6) \times 10^{-16}$
	Cis-cyclooctene	2	304 ± 1	1.0 ± 0.1	$(3.8 \pm 0.4) \times 10^{-16}$
				$k=(4.2 \pm 1.0) \times 10^{-16}$ cm^3 molecule^{-1} s^{-1}	

were placed on an absolute basis using the following rate constants: $k(cis\text{-cyclooctene}+O_3)=3.86 \times 10^{-16}$ cm^3 molecule^{-1} s^{-1} (Cusick & Atkinson, 2005) and $k(cyclohexene+O_3)=8.1 \times 10^{-17}$ cm^3 molecule^{-1} s^{-1} (Calvert et al., 2000). The rate constants for the studied reactions derived from this study at 303 ± 2 K and 760 Torr of purified air are (in cm^3 molecule^{-1} s^{-1})

$$\alpha\text{-pinene}+O_3 \rightarrow \text{Products} \quad k = (9.6 \pm 1.6) \times 10^{-17}$$
$$\text{sabinene}+O_3 \rightarrow \text{Products} \quad k = (8.4 \pm 1.3) \times 10^{-17}$$
$$\text{limonene}+O_3 \rightarrow \text{Products} \quad k = (2.0 \pm 0.4) \times 10^{-16}$$
$$\text{myrcene}+O_3 \rightarrow \text{Products} \quad k = (4.2 \pm 1.0) \times 10^{-16}$$
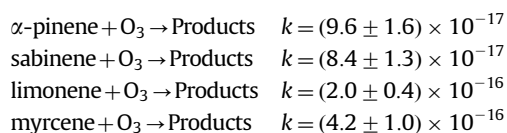
The quoted errors on the rate constants values result from the error from the rate constant ratios (one-standard deviation, 1σ) and do not include the error of the reference rate constant. As a support for these previous measurements, decay rates of cyclohexene versus that of *cis*-cyclooctene were also determined from two consecutive runs leading to a rate constant ratio of $k(cyclohexene+O_3)/k(cis\text{-cyclooctene}+O_3)=0.20 \pm 0.03$. This value is in excellent agreement with the rate constant ratio of $k(cyclohexene+O_3)/k(cis\text{-cyclooctene}+O_3)=0.21$ used here.

4.1.3. Comparison with literature
The rate constants values obtained in this work using both facilities (simulation chamber and flow tube) are compared with the existing data in the literature in Table 3. Recommendations from Calvert et al. (2000) and Atkinson et al. (2006) are also included for comparison. The rate constants measured with the two methods in our laboratory are in agreement except for that of the reaction of ozone with limonene for which the value obtained using the simulation chamber is almost factor two lower than that derived from the flow reactor study. For the reactions of ozone with α-pinene, sabinene and myrcene, a good agreement is also generally observed between the measurement reported here and those from the literature. No evident explanation could be given for the observed difference between the $k(O_3+\text{limonene})$ obtained using the two techniques. The value derived from the simulation chamber study is in agreement with the literatures data.

4.2. From particle counting to nucleation threshold

Experiments were performed at $T \sim 296$ K and $P \sim 764$ Torr under dry conditions (dew point ≤ -33 °C), in the absence of any seed particles and no OH radical scavenger has been added to the gas mixture. Particles were formed under the initial concentrations of $[\text{monoterpenes}]_0=(0.75-5.1) \times 10^{13}$ molecules cm^{-3} and $[O_3]_0=(0.25-3.5) \times 10^{12}$ molecules cm^{-3}, and reaction time ranging from 17 to 48 s with a total flow rate maintained at 4.6 L min^{-1}. Ozone was continuously measured with an ultra-violet monitor at the outlet of the reactor. The initial conditions imply that ozone concentration is homogeneous all over the flow section as well as particle number concentration. Therefore, we assume that no radical gradient is generated limiting diffusion processes of particles. Particle number concentration has been measured continuously at the outlet of the flow reactor with a Condensation Particle Counter (CPC Model 3022A, TSI) operating with a flow rate of 1.25 L min^{-1} and acquisition time adjusted from 1 to 5 s. In this work, the detection limit in terms of particle number concentration of the CPC3022A has been estimated based on the variability of the CPC signal during off-experiments (in the absence of monoterpenes and in the presence of ozone only). In our experimental conditions, a value of 0.3 particles cm^{-3} (equivalent to three-standard deviations) has been found where experiments leading to a particle number below this limit were not cited in the final results.

Table 3
Rate constants values for the reactions of ozone with the investigated monoterpenes: the data obtained in this work and those from the literature.

Reaction	Rate constant, k (cm^3 molecule^{-1} s^{-1})	T (K)	Reference
α-Pinene$+O_3$	$(11 \pm 1) \times 10^{-17}$	296 ± 1	This work (flow reactor)
	$(9.6 \pm 1.6) \times 10^{-17}$	302 ± 1	This work (smog chamber)
	$(9.0 \pm 0.6) \times 10^{-17}$	303.2 ± 0.1	Tillmann et al. (2009)
	$(9.0 \pm 1.8) \times 10^{-17}$	298	Atkinson et al. (2006)
	$(10.6 \pm 0.9) \times 10^{-17}$	295	Witter et al. (2002)
	$(8.41 \pm 0.74) \times 10^{-17}$	298	Khamaganov & Hites (2001)
	$(9.71 \pm 1.06) \times 10^{-17}$	296 ± 2	Atkinson et al. (1990a)
	$(8.20 \pm 1.24) \times 10^{-17}$	297 ± 2	Nolting et al. (1988)
	$(8.4 \pm 1.9) \times 10^{-17}$	296 ± 2	Atkinson et al. (1982)
	14.5×10^{-17}	295 ± 1	Grimsrud et al. (1975)
	$(33 \pm 3) \times 10^{-17}$	298	Japar et al. (1974)
	16×10^{-17}	294	Ripperton et al. (1972)
Sabinene$+O_3$	$(6.2 \pm 2.1) \times 10^{-17}$	297 ± 1	This work (flow reactor)
	$(8.4 \pm 1.3) \times 10^{-17}$	303 ± 2	This work (smog chamber)
	$(8.3 \pm 2.5) \times 10^{-17}$	298	Calvert et al. (2000)
	$(8.61 \pm 0.94) \times 10^{-17}$	296 ± 2	Atkinson et al. (1990a)
	$(8.07 \pm 0.83) \times 10^{-17}$	296 ± 2	Atkinson et al. (1990b)
Limonene$+O_3$	$(3.8 \pm 0.3) \times 10^{-16}$	297 ± 1	This work (flow reactor)
	$(2.0 \pm 0.4) \times 10^{-16}$	304 ± 2	This work (smog chamber)
	$(2.5 \pm 0.3) \times 10^{-16}$	295	Witter et al. (2002)
	$(2.13 \pm 0.15) \times 10^{-16}$	298	Khamaganov & Hites (2001)
	$(2.0 \pm 0.5) \times 10^{-16}$	298	Calvert et al. (2000)
	$(2.01 \pm 0.07) \times 10^{-16}$	296 ± 2	Shu & Atkinson (1994)
	3.5×10^{-16}	297.3	Zhang et al. (1994)
	$(2.09 \pm 0.22) \times 10^{-16}$	296 ± 1	Atkinson et al. (1990a)
	6.49×10^{-16}	295 ± 1	Grimsrud et al. (1975)
Myrcene$+O_3$	$(5.7 \pm 1.6) \times 10^{-16}$	298 ± 1	This work (flow reactor)
	$(4.2 \pm 1.0) \times 10^{-16}$	304 ± 2	This work (smog chamber)
	$(3.85^{+0.29}_{-0.27}) \times 10^{-16}$	298	Daekyun et al. (2011)
	$(4.8 \pm 0.6) \times 10^{-16}$	295	Witter et al. (2002)
	$(4.85 \pm 0.78) \times 10^{-16}$	296 ± 2	Atkinson et al. (1990a)
	12.5×10^{-16}	295 ± 1	Grimsrud et al. (1975)

The concentration of consumed monoterpenes (Δ[monoterpene]) has been calculated according to the decrease of the ozone concentration based on the kinetic pseudo-first order conditions ([monoterpene]$_0 \gg$ [O$_3$]$_0$) as follows:

$$\Delta[O_3] = [O_3]_0 \times (1 - \exp(-k[\text{monoterpene}]_0 t)) \tag{3}$$

It is known that the reaction of ozone with the investigated monoterpenes leads to the formation of OH radicals (33–80%) (Atkinson et al., 1992, 2006; Aschmann et al., 2002). This had to be taken account since OH is highly reactive towards these monoterpenes and hence may contribute to their total loss in our experimental system (k(monoterpenes$+$OH)$=(0.5-2) \times 10^{-10}$ cm^3 molecule^{-1} s^{-1} (Atkinson et al., 1986, 1990b, 2006). Consequently, the calculation of the consumed concentration of monoterpene, Δ[monoterpene], has been calculated according to

$$\Delta[\text{monoterpene}] = (1 + \alpha_{OH}) \times \Delta[O_3] \tag{4}$$

with α_{OH}, the OH formation yield from the ozonolysis reaction. Estimation of standard deviation of the consumed concentration of monoterpene, $\sigma_{\Delta[\text{monoterpene}]}$, for a time t is established as follows:

$$\sigma_{\Delta[\text{monoterpene}]} = \Delta[O_3] \times (\sigma_{\alpha_{OH}} + (1 + \alpha_{OH}) \times (A + B)) \tag{5}$$

with $A = \dfrac{\sigma_{[O_3]_0}}{[O_3]_0}$ and $B = \left(\dfrac{k[\text{monoterpene}]_0 t}{\exp(k[\text{monoterpene}]_0 t) - 1} \right) \times \left(\dfrac{\sigma_k}{k} + \dfrac{\sigma_{[\text{monoterpene}]_0}}{[\text{monoterpene}]_0} + \dfrac{\sigma_t}{t} \right)$

where $\sigma_{\alpha_{OH}}$, $\sigma_{[O_3]0}$, σ_k and σ_t are the corresponding standard deviations for the OH formation yield, the initial concentration of ozone, the rate constant of ozonolysis reaction and the reaction time, respectively. The rate constants of the ozonolysis reactions used to estimate the consumed fraction of monoterpene are based on the present study and OH radical formation yields are for α-pinene (0.80 ± 0.12) taken from IUPAC recommendation (Atkinson et al., 2006), and for sabinene (0.33 ± 0.05), limonene (0.67 ± 0.10) and myrcene (0.63 ± 0.09), values are extracted from Aschmann et al. (2002). Therefore, aerosols observed in our system could be due to the reaction of monoterpenes with both ozone and OH radicals. We have estimated that the contribution of OH radicals to the consumption rate of monoterpene represents up to 44% for α-pinene, 25% for sabinene, 40% for limonene and 39% for myrcene.

Fig. 8 shows a typical number concentration of particles formed over the course of α-pinene ozonolysis reaction. Ozone is introduced first in the flow reactor and the particle background monitored for at least 3 h. The particle number increases few minutes after the addition of the monoterpene to the gas mixture in the reactor. This delay might be attributed to a treatment of the inner reactor surface. Once this "treatment" completed, the number concentration of particles (N) reaches a levelling-off maintained constant during the course of the run. Between two runs, the flow reactor is cleaned up by flowing ozone until a residual concentration of particles of 10^{-2}–10^{-1} particles cm^{-3}. For any wall loss, particles should displace for a distance of 3.15 cm from the sampling orifice for a sampling flow of 1.25 L min^{-1}. With a diffusion coefficient of particles, $D = 5.5 \times 10^{-4}$ cm^2 s^{-1} for a particle size distribution centred at 10 nm (Baron & Willeke, 2001) and the maximum residence time $t = 48$ s, particles will displace only for a distance of 0.23 cm which makes diffusion losses not significant in our system. In addition, coagulation process affects particle number concentration over a period of time according to $N_t = N_0/(1 + N_0 K t)$, with N_0 and N_t the number of particles (cm^{-3}) at times t_0 and t, respectively, and K, the coagulation coefficient (cm^{-3} s^{-1}). Using $K = 9 \times 10^{-10}$ cm^3 s^{-1} for a size particle diameter centred at 10 nm (Seinfeld & Pandis, 1998), under the most unfavourable conditions ($t = 48$ s and $N_0 = 10^6$ particles cm^{-3}), it has been found that 4% of the particle number concentration will be lost by coagulation process. It should be mentioned that as lower the residence time and aerosol production are, coagulation process becomes negligible. No surface artefact for ozone reaction has been observed in contrary to the reactions of OH and NO$_3$ radicals (Bonn & Moortgat, 2002).

Number concentrations of SOA have been measured for different initial concentrations of the reactants and consumed concentrations of monoterpenes. The number of particles formed for an experiment results from the average obtained from 5 to 15 min time interval associated with a one-standard deviation (1σ) as given in Table 4 for α-pinene. Reacted
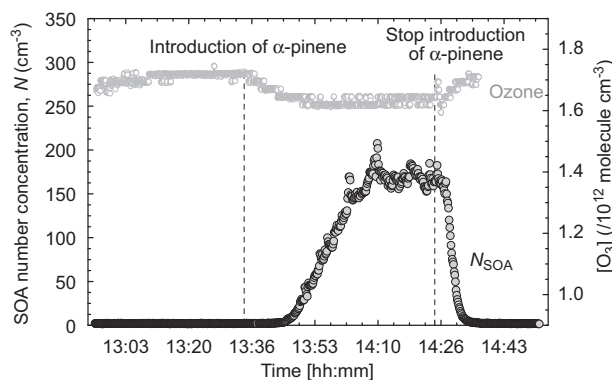

Fig. 8. Example of SOA formation produced from the ozonolysis of α-pinene ([α-pinene]$_0$ = 9.8×10^{12} molecules cm^{-3}) in the flow reactor ($t = 17$ s).

Table 4
Initial conditions and the results obtained on particle formation studied from the ozonolysis of α-pinene (no OH scavenger has been used) at 296 ± 1 K and 764.4 ± 0.3 Torr.

Exp.	T (K)	[α-pinene]$_0$/10^{13} (molecule cm^{-3})	[O$_3$]$_0$/10^{12} (molecule cm^{-3})	t (s)	Δ[α-pinene]/10^{10} (molecule cm^{-3})	$N \pm 1\sigma$ (cm^{-3})
1	295.0	5.11	3.30	48 ± 2	124.7 ± 43.1	$(9.91 \pm 0.28) \times 10^5$
2	295.2	5.10	3.41	36 ± 2	99.1 ± 36.5	$(2.00 \pm 0.06) \times 10^6$
3	295.4	5.08	3.46	17 ± 1	49.6 ± 19.0	$(4.10 \pm 0.03) \times 10^5$
4	296.1	2.83	1.20	48 ± 2	26.5 ± 9.6	$(2.80 \pm 0.08) \times 10^5$
5	296.0	2.83	1.22	26 ± 1	15.0 ± 5.6	$(8.96 \pm 0.12) \times 10^4$
6	297.1	1.52	1.75	26 ± 1	11.7 ± 4.3	$(1.68 \pm 0.08) \times 10^3$
7	294.5	1.71	1.14	26 ± 1	8.6 ± 3.2	$(6.71 \pm 0.23) \times 10^3$
8	295.7	1.70	1.30	23 ± 1	8.6 ± 3.2	$(6.35 \pm 0.19) \times 10^3$
9	297.1	1.50	1.85	17 ± 1	8.0 ± 3.2	$(2.95 \pm 0.04) \times 10^3$
10	296.9	0.98	1.87	23 ± 1	7.2 ± 2.7	$(2.46 \pm 0.04) \times 10^3$
11	297.3	1.12	1.02	26 ± 1	5.1 ± 1.9	139 ± 3
12	295.0	0.98	1.73	17 ± 1	5.0 ± 2.0	168 ± 10
13	294.9	0.99	1.48	20 ± 1	5.0 ± 2.0	4 ± 1
14	295.5	0.98	1.61	17 ± 1	4.6 ± 1.8	34 ± 2
15	297.2	1.03	1.03	21 ± 1	3.8 ± 1.5	13.5 ± 0.5
16	297.5	1.03	1.00	20 ± 1	3.5 ± 1.4	0.34 ± 0.10
17	295.9	0.98	1.00	19 ± 1	3.2 ± 1.3	5.14 ± 0.62
18	296.3	0.98	0.99	18 ± 1	3.0 ± 1.2	4.94 ± 0.52
19	296.9	0.98	0.99	18 ± 1	3.0 ± 1.2	0.32 ± 0.18
20	295.7	0.98	0.91	19 ± 1	2.9 ± 1.1	42 ± 4
21	295.7	0.98	0.97	17 ± 1	2.8 ± 1.1	0.76 ± 0.48

monoterpenes concentration ranged from 4.5×10^9 to 1.25×10^{12} molecule cm^{-3}. Uncertainty (one-standard deviation, 1σ) on the consumed fraction of monoterpene on the whole studied monoterpenes ranges from 22% to 61%. The profiles of particle formation efficiency versus the consumed concentration of monoterpenes ($\log N = f(\Delta[\text{monoterpene}])$) are displayed in Figs. 9–12. The data obtained are compared with the existing ones reported in the literature (Koch et al., 2000; Berndt et al., 2003; Bonn & Moortgat, 2003; Lee & Kamens, 2005). The results of Koch et al. (2000) were based on simulation chamber experiment whereas those of Berndt et al. (2003) and Lee & Kamens (2005) were performed in flow reactor. The obtained data from Koch et al. (2000) have been compared using the same rate constants and OH formation yields as those used in this work.

For all studied monoterpenes, number concentration of particles formed increases exponentially for higher consumed fraction of monoterpenes and reaches a plateau around 10^5–10^6 particles cm^{-3}. Fig. 13 compares the SOA formation efficiency for a low consumption of monoterpene. It appears that among the studied monoterpenes, sabinene and limonene have higher SOA formation potential than myrcene and α-pinene.

Nucleation thresholds for each monoterpene were extracted from the plot of $\log N = f(\Delta[\text{monoterpene}])$, summarised in Table 5 and compared to the existing data from literature. The nucleation thresholds are given as upper limits obtained from the lowest amount of consumed monoterpene for which particles were observed, where its absolute error is added. As given in Table 5, the nucleation threshold values obtained here were found to be lower than the previously reported
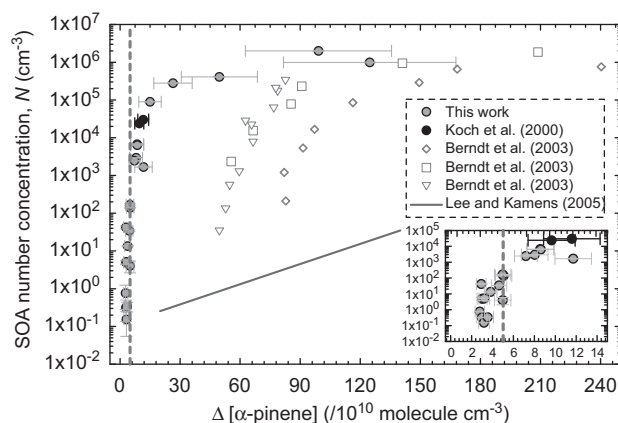

Fig. 9. Particle number formed as function of consumed concentration of α-pinene through reaction with ozone. Dotted line corresponds to the nucleation threshold calculated by Bonn & Moortgat (2003) (5.0×10^{10} molecule cm^{-3}). Results of Berndt et al. (2003) are obtained for initial concentration of α-pinene (in molecule cm^{-3}): ($\diamond$) 1.75×10^{13}, ($\square$) 4.4×10^{12} and ($\triangledown$) 1.2×10^{12}. The inserted graph shows a zoom from low concentrations of consumed α-pinene.
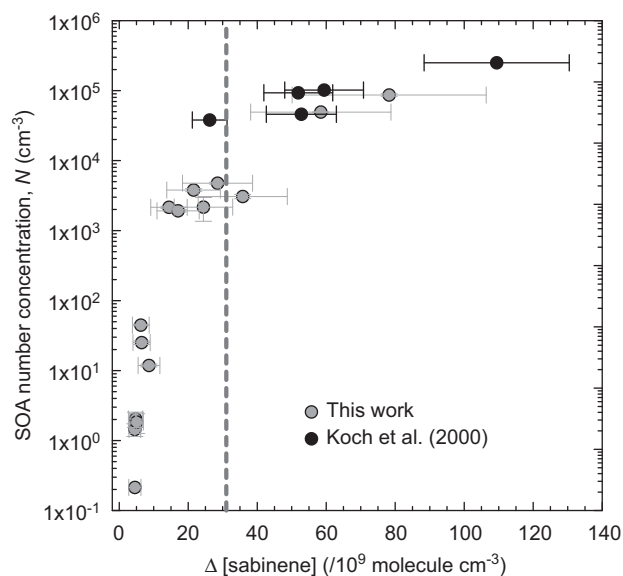

Fig. 10. Particle number formed as function of consumed concentration of sabinene through reaction with ozone. Dotted line corresponds to the nucleation threshold calculated by Bonn & Moortgat (2003) (3.1×10^{10} molecule cm^{-3}).
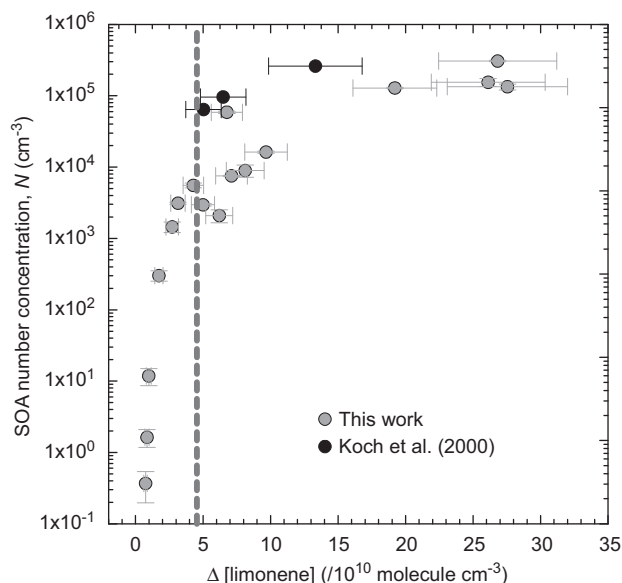
Fig. 11. Particle number formed as function of consumed concentration of limonene through reaction with ozone. Dotted line corresponds to the nucleation threshold calculated by Bonn & Moortgat (2003) (4.5×10^{10} molecule cm^{-3}).
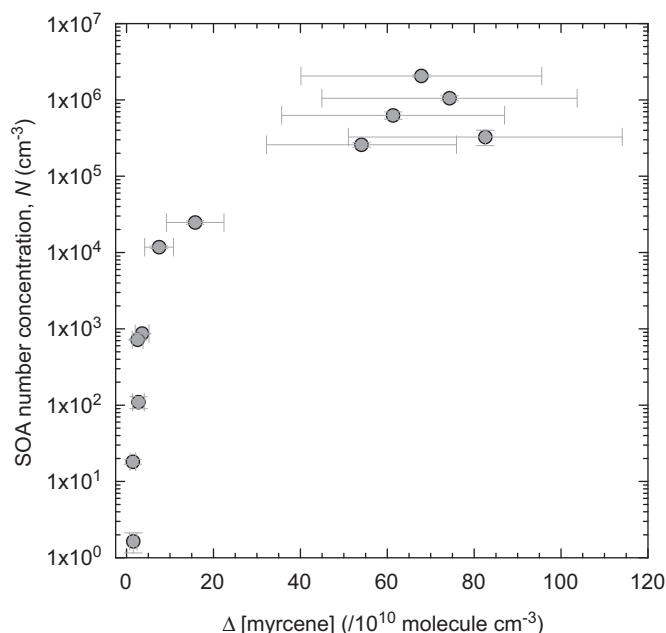

Fig. 12. Particle number formed as function of consumed concentration of myrcene through reaction with ozone.

ones for α-pinene, sabinene and limonene (Koch et al., 2000; Berndt et al., 2003; Bonn & Moortgat, 2003; Lee & Kamens, 2005). However, it has to be underlined that the interpretation of the data has to take into account the type of CPCs used in different studies since they may have serious variations in the cutoff sizes. This work provides the first result for SOA counting from the ozonolysis of myrcene.

The value given by Bonn & Moortgat (2003) originated from the FACSIMILE model based on the experimental results of Koch et al. (2000). Koch et al. (2000) used a CPC Model 3010 (D_{50}=10.9 nm, (Heim et al., 2004)) whereas Berndt et al. (2003) used a UCPC Model 3025 (D_{50}=3.1 nm, (Kesten et al., 1991)). The determination of the 50% counting efficiency diameter (D_{50}) was performed using NaCl aerosol. Indeed, the use of ultrafine particle counter such as 3025 model which has a particle cutoff diameter (D_{50}) of 3.1 nm would allow to measure higher number of particles and for lower consumed concentration of monoterpenes (and the nucleation threshold). As shown in Table 5, a disagreement is observed between
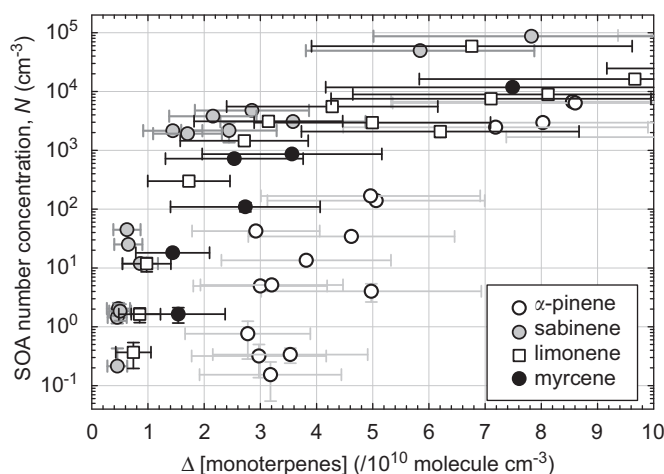
Fig. 13. Comparison of SOA number concentration formed in the flow reactor from the ozonolysis of α-pinene, sabinene, limonene and myrcene for low concentration of consumed monoterpene.

Table 5
Values of nucleation thresholds obtained from SOA particle counting from the ozonolysis of monoterpenes performed in the flow reactor. Experiments were performed at $T \sim 296$ K, $P \sim 764$ Torr and dew point ≤ -33 °C, in the absence of any OH scavenger and seed particles.

Monoterpenes	Structure	SOA nucleation thresholds (molecule cm^{-3} (ppb))	Reference
α-Pinene		3.9×10^{10} (1.56)	This work
		5.0×10^{10} (2.1)[a]	Bonn & Moortgat (2003)[a]
		3×10^{11} (12)	Berndt et al. (2003)
Sabinene		6.2×10^{9} (0.26)	This work
		3.1×10^{10} (1.3)[a]	Bonn & Moortgat (2003)[a]
Limonene		1.1×10^{10} (0.43)	This work
		4.5×10^{10} (1.9)[a]	Bonn & Moortgat (2003)[a]
Myrcene		2.1×10^{10} (0.83)	This work

[a] Calculated value from the experiments of Koch et al. (2000); Koch et al. (2000) used a CPC Model 3010 (D_{50}=10.9 nm, (Heim et al., 2004)); Berndt et al. (2003) used a UCPC Model 3025 (D_{50}=3.1 nm, (Kesten et al., 1991)). In the present work, we used a CPC Model 3022A (D_{50}=8.3 nm, (Ankilov et al., 2002)).

the nucleation thresholds reported in different studies. This could be at least partly due the use of different models of CPCs (the one used in this work is Model 3022A, D_{50}=8.3 nm, (Ankilov et al., 2002)). Another explanation for this disagreement is the use of wide range of alkene/ozone ratios. Indeed, this work has been performed under initial ratio of 5–43 whereas the previous studies were: Koch et al. (2000), 0.02–1.23; Berndt et al. (2003), 0.3–1.6; Lee & Kamens (2005), 12–51. As reported, alkene/ozone ratio could control the concentration of transient species (i.e. RO$_2$) which are known to play a key role in particle formation (Wolf et al., 2009).

The nucleation threshold from the ozonolysis of α-pinene obtained in this work (3.9×10^{10} molecule cm^{-3}) is in good agreement with that reported by Bonn & Moortgat (2003) (5.0×10^{10} molecule cm^{-3}). Berndt et al. (2003) proposed 3×10^{11} molecule cm^{-3} as a conversion limit. It should be noted that Berndt et al. (2003) observed a dependence of the conversion limit with the initial concentration of α-pinene which remains unexplained so far. Moreover, the results from this work show the same trend as from the data reported by Bonn & Moortgat (2003) for α-pinene, sabinene and limonene. Therefore, monoterpenes can be ordered with respect to their SOA formation potential: α-pinene < myrcene < limonene < sabinene. The results from this study indicate that sabinene is the most important SOA precursor among the studied monoterpenes in contrast to α-pinene which is the least efficient in the SOA formation.

5. Conclusions

The aerosol flow reactor recently developed in our laboratory combined to a CPC has been used to study the secondary organic aerosol formation during the ozonolysis of a series of monoterpenes (α-pinene, sabinene, limonene and myrcene). The experiments were conducted in absence of OH radical scavenger and seed particles. The data obtained enabled us to evaluate the aerosol formation thresholds which were compared with the existing literature data. The present work constitutes the first study on the aerosol formation threshold through the ozonolysis of myrcene and reports threshold values lower than those obtained in previous investigations for the ozonolysis of α-pinene, sabinene and limonene. The nucleation thresholds determined here were found to be ≤ 1.6 ppb and the trend observed for the studied monoterpenes agrees with that observed in the literature (Bonn & Moortgat, 2003).

However, the sensitivity of the particle counters used in this type of work is one of the limited criteria in the accuracy of the assessment of nucleation thresholds. Indeed, it should be mentioned that, nucleation threshold is apprehended as an observation threshold where atmospheric particles nucleate with a particle size diameter lower than 3 nm and the particle cutoff diameter of CPC used (D_{50}=8.3 nm, (Ankilov et al., 2002)). Accurate conversion limit data could be obtained by more sensitive particle counter by the use for example of ion mobility spectrometers which can be extended to 0.4 nm corresponding to molecular ion range diameter (Kulmala et al., 2004a).

Using the set-up developed in our laboratory, future work will consist in evaluating the dependence of SOA nucleation threshold in more realistic conditions (e.g. at different relative humidity, in presence of other species such as NO$_X$ and SO$_2$). These parameterizations using experimental data would be necessary in evaluating the VOC contribution to SOA formation in remote and polluted areas and further to enrich air quality models.

Acknowledgements

References

Ankilov, A., Baklanov, A., Colhoun, M., Enderle, K.H., Gras, J., Julanov, Y., Kaller, D., Lindner, A., Lushnikov, A.A., Mavliev, R., McGovern, F., O'Connor, T.C., Podzimek, J., Preining, O., Reischl, G.P., Rudolf, R., Sem, G.J., Szymanski, W.W., Vrtala, A.E., Wagner, P.E., Winklmayr, W., & Zagaynov, V. (2002). Particle size dependent response of aerosol counters. *Atmospheric Research*, 62, 209–237.

Aschmann, S.M., Arey, J., & Atkinson, R. (2002). OH radical formation from the gas-phase reactions of O$_3$ with a series of terpenes. *Atmospheric Environment*, 36, 4347–4355.

Atkinson, R., Winer, A.M., & Pitts, J.N., Jr. (1982). Rate constants for the gas phase reactions of O$_3$ with the natural hydrocarbons isoprene and α- and β-pinene. *Atmospheric Environment*, 16, 1017–1020.

Atkinson, R., Aschmann, S.M., & Pitts, J.N., Jr. (1986). Rate constants for the gas-phase reactions of the OH radical with a series of monoterpenes at 294 ± 1 K. *International Journal of Chemical Kinetics*, 18, 287–299.

Atkinson, R., Hasegawa, D., & Aschmann, S.M. (1990a). Rate constants for the gas-phase reactions of O$_3$ with a series of monoterpenes and related compounds at 296 ± 2 K. *International Journal of Chemical Kinetics*, 22, 871–887.

Atkinson, R., Aschmann, S.M., & Arey, J. (1990b). Rate constants for reactions of OH and NO$_3$ radicals and O$_3$ with sabinene and camphene at 296 ± 2 K. *Atmospheric Environment*, 24A, 2647–2654.

Atkinson, R., Aschmann, S.M., Arey, J., & Shorees, B. (1992). Formation of OH radicals in the gas phase reactions of O$_3$ with a series of terpenes. *Journal of Geophysical Research*, 97, 6065–6073.

Atkinson, R., & Arey, J. (2003). Gas-phase tropospheric chemistry of biogenic volatile organic compounds: a review. *Atmospheric Environment*, 37, S197–S219.

Atkinson, R., Baulch, D.L., Cox, R.A., Crowley, J.N., Hampson, R.F., Hynes, R.G., Jenkin, M.E., Rossi, M.J., & Troe, J. (2004). Evaluated kinetic and photochemical data for atmospheric chemistry: Volume I—gas phase reactions of O$_x$, HO$_x$, NO$_x$ and SO$_x$ species. *Atmospheric Chemistry and Physics*, 4, 1461–1738.

Atkinson, R., Baulch, D.L., Cox, R.A., Crowley, J.N., Hampson, R.F., Hynes, R.G., Jenkin, M.E., Rossi, M.J., & Troe, J. (2006). Evaluated kinetic and photochemical data for atmospheric chemistry: Volume II—gas phase reactions of organic species. *Atmospheric Chemistry and Physics*, 6, 3625–4055.

Baker, J., Arey, J., & Atkinson, R. (2004). Kinetics of the gas-phase reactions of OH radicals, NO$_3$ radicals and O$_3$ with three C7-carbonyls formed from the atmospheric reactions of myrcene, ocimene and terpinolene. *Journal of Atmospheric Chemistry*, 48(3), 241–260.

Baron, P.A., & Willeke, B. (2001). *Aerosol measurements: principles, techniques, and applications* (2nd edition). ISBN: 0-471-35636-0.

Bernard, F., Eglunent, G., Daële, V., & Mellouki, A. (2010). Kinetics and products of the gas-phase reactions of ozone with methyl methacrylate, methyl acrylate and ethyl acrylate. *Journal of Physical Chemistry A*, 114(32), 8376–8383.

Berndt, T., Böge, O., & Stratmann, F. (2003). Gas-phase ozonolysis of α-pinene: gaseous products and particle formation. *Atmospheric Environment*, 37, 3933–3945.

Bonn, B., & Moortgat, G.K. (2002). New particle formation during α- and β-pinene oxidation by O₃, OH and NO₃, and the influence of water vapour: particle size distribution studies. *Atmospheric Chemistry and Physics*, 2, 183–196.

Bonn, B., & Moortgat, G.K. (2003). Sesquiterpene ozonolysis: origin of atmospheric new particle formation from biogenic hydrocarbons. *Geophysical Research Letters*, 30(11), 1585.

Burkholder, J.B., Curtius, J., Ravishankara, A.R., & Lovejoy, E.R. (2004). Laboratory studies of the homogeneous nucleation of iodine oxides. *Atmospheric Chemistry and Physics*, 4, 19–34.

Burkholder, J.B., Baynard, T., Ravishankara, A.R., & Lovejoy, E.R. (2007). Particle nucleation following the O₃ and OH initiated oxidation of α-pinene and β-pinene between 278 and 320 K. *Journal of Geophysical Research*, 112, D10216.

Calogirou, A., Jensen, N.R., Nielsen, C.J., Kotzias, D., & Hjorth, J. (1999). Gas-phase reactions of nopinone, 3-isopropenyl-6-oxo-heptanal, and 5-methyl-5-vinyltetrahydrofuran-2-ol with OH, NO₃, and ozone. *Environmental Science and Technology*, 33(3), 453–460.

Calvert, J.G., Atkinson, R., Kerr, J.A., Madronich, S., Moortgat, G.K., Wallington, T.J., & Yarwood, G. (2000). *The mechanisms of atmospheric oxidation of the alkenes*. Oxford University Press: New York.

Cocker, D.R., III, Clegg, S.L., Flagan, R.C., & Seinfeld, J.H. (2001a). The effect of water on gas–particle partitioning of secondary organic aerosol. Part I: α-pinene/ozone system. *Atmospheric Environment*, 35, 6049–6072.

Cocker, D.R., III, Mader, B.T., Kalberer, M., Flagan, R.C., & Seinfeld, J.H. (2001b). The effect of water on gas–particle partitioning of secondary organic aerosol: II. m-xylene and 1,3,5-trimethylbenzene photooxidation systems. *Atmospheric Environment*, 35, 6073–6085.

Cusick, R.D., & Atkinson, R. (2005). Rate constants for the gas-phase reactions of O₃ with a series of cycloalkenes at 296 ± 2 K. *International Journal of Chemical Kinetics*, 37, 183–190.

Daekyun, K., Stevens, P.S., & Hites, R.A. (2011). Rate constants for the gas phase reactions with OH and O₃ with β-ocimene, β-myrcene, and α- and β-farnesene as a function of temperature. *Journal of Physical Chemistry A*, 115(4), 500–506.

Enghoff, M.B., & Svensmark, H. (2008). The role of atmospheric ions in aerosol nucleation—a review. *Atmospheric Chemistry and Physics*, 8, 4911–4923.

Griffin, R.J., Cocker, D.R., III, Flagan, R.C., & Seinfeld, J.H. (1999). Organic aerosol formation from the oxidation of biogenic hydrocarbons. *Journal of Geophysical Research*, 104, 3555–3567.

Grimsrud, E.P., Westberg, H.H., & Rasmussen, R.A. (1975). Atmospheric reactivity of monoterpene hydrocarbons, NOₓ photooxidation and ozonolysis. *International Journal of Chemical Kinetics Symposium*, 1, 183.

Guenther, A., Hewitt, N.C., Erickson, D., Fall, R., Geron, C., Graedel, T., Harley, P., Klinger, L., Lerdau, M., McKay, W.A., Pierce, T., Scholes, B., Steinbrecher, R., Tallamraju, P., Taylor, J., & Zimmerman, P. (1995). A global model of natural volatile organic compound emissions. *Journal of Geophysical Research*, 100, 8873–8892.

Hallquist, M., Wenger, J.C., Baltensperger, U., Rudich, Y., Simpson, D., Claeys, M., Dommen, J., Donahue, N.M., George, C., Goldstein, A.H., Hamilton, J.F., Herrmann, H., Hoffmann, T., Iinuma, Y., Jang, M., Jenkin, M.E., Jimenez, J.L., Kiendler-Scharr, A., Maenhaut, W., McFiggans, G., Mentel, T.F., Monod, A., Prévôt, A.S.H., Seinfeld, J.H., Surratt, J.D., Szmigielski, R., & Wildt, J. (2009). The formation, properties and impact of secondary organic aerosol: current and emerging issues. *Atmospheric Chemistry and Physics*, 9, 5155–5235.

Heim, M., Kasper, G., Reischl, G.P., & Gerhart, C. (2004). Performance of a new commercial electrical mobility spectrometer. *Aerosol Science and Technology*, 38, 3–14.

Hoffmann, T., Odum, J.R., Bowman, F., Collins, D., Klockow, D., Flagan, R.C., & Seinfeld, J.H. (1997). Formation of organic aerosols from the oxidation of biogenic hydrocarbons. *Journal of Atmospheric Chemistry*, 26, 189–222.

Hoppel, W., Fitzgerald, J., Frick, G., Caffrey, P., Pasternack, L., Hegg, D., Gao, S., Leaitch, R., Shantz, N., Cantrell, C., Albrechcinski, T., Ambrusko, J., & Sullivan, W. (2001). Particle formation and growth from ozonolysis of α-pinene. *Journal of Geophysical Research*, 106, 27603–27618.

Japar, S.M., Wu, C.H., & Niki, H. (1974). Rate constants for the gas phase reaction of ozone with α-pinene and terpinolene. *Environmental Letters*, 7, 245–249.

Jonsson, Ä., Hallquist, M., & Ljungström, E. (2006). Impact of humidity on the ozone Initiated oxidation of limonene, Δ3-carene, and α-pinene. *Environmental Science and Technology*, 40, 188–194.

Jonsson, Ä., Hallquist, M., & Ljungström, E. (2008a). Influence of OH scavenger on the water effect on secondary organic aerosol formation from ozonolysis of limonene, Δ³-carene, and α-pinene. *Environmental Science and Technology*, 42, 5938–5944.

Jonsson, Ä., Hallquist, M., & Ljungström, E. (2008b). The effect of temperature and water on secondary organic aerosol formation from ozonolysis of limonene, Δ³-carene and α-pinene. *Atmospheric Chemistry and Physics*, 8, 6541–6549.

Kanakidou, M., Seinfeld, J.H., Pandis, S.N., Barnes, I., Dentener, F.J., Facchini, M.C., Van Dingenen, R., Ervens, B., Nenes, A., Nielsen, C.J., Swietlicki, E., Putaud, J.P., Balkanski, Y., Fuzzi, S., Horth, J., Moortgat, G.K., Winterhalter, R., Myhre, C.E.L., Tsigaridis, K., Vignati, E., Stephanou, E.G., & Wilson, J. (2005). Organic aerosol and global climate modelling: a review. *Atmospheric Chemistry and Physics*, 5, 1053–1123.

Kaufman, F. (1984). Kinetics of elementary radical reactions in the gas phase. *Journal of Physical Chemistry*, 88, 4909–4917.

Kavouras, I.G., & Stephanou, E.G. (2002). Direct evidence of atmospheric secondary organic aerosol formation in forest atmosphere through heteromolecular nucleation. *Environmental Science and Technology*, 36, 5083–5091.

Kesten, J., Reineking, A., & Porstendörfer, J. (1991). Calibration of a TSI Model 3025 ultrafine condensation particle counter. *Aerosol Science and Technology*, 15, 107–111.

Khamaganov, V.G., & Hites, R.A. (2001). Rate constants for the gas-phase reactions of ozone with isoprene, a- and b-Pinene, and limonene as a function of temperature. *Journal of Physical Chemistry A*, 105, 815–822.

Koch, S., Winterhalter, R., Uherek, E., Kolloff, A., Neeb, P., & Moortgat, G.K. (2000). Formation of new particles in the gas-phase ozonolysis of monoterpenes. *Atmospheric Environment*, 34, 4031–4042.

Kroll, J.H., Ng, N.L., Murphy, S.M., Flagan, R.C., & Seinfeld, J.H. (2006). Secondary organic aerosol formation from isoprene photooxidation. *Environmental Science and Technology*, 40, 1869–1877.

Kulmala, M., & Laaksonen, A. (1990). Binary nucleation of water-sulfuric acid system: comparison of classical theories with different H₂SO₄ saturation vapor pressures. *Journal of Physical Chemistry*, 93, 696–701.

Kulmala, M., Pirjola, L., & Mäkelä, J.M. (2000). Stable sulphate clusters as a source of new atmospheric particles. *Nature*, 404, 66–69.

Kulmala, M., Vehkamäki, H., Petäjä, T., Dal Maso, M., Lauri, A., Kerminen, V.-M., Birmili, W., & McMurry, P.H. (2004a). Formation and growth rates of ultra-fine atmospheric particles: a review of observations. *Journal of Aerosol Science*, 35, 143–176.

Kulmala, M., Kerminen, V.-M., Anttila, T., Laaksonen, A., & O'Dowd, C.D. (2004b). Organic aerosol formation via sulphate cluster activation. *Journal of Geophysical Research*, 109, D04205.

Lee, A., Goldstein, A.H., Keywood, M.D., Gao, S., Varutbangkul, V., Bahreini, R., Ng, N.L., Flagan, R.C., & Seinfeld, J.H. (2006a). Gas-phase products and secondary aerosol yields from the ozonolysis of ten different terpenes. *Journal of Geophysical Research*, 111, 1–18.

Lee, A., Goldstein, A.H., Kroll, J.H., Ng, N.L., Varutbangkul, V., Flagan, R.C., & Seinfeld, J.H. (2006b). Gas-phase products and secondary aerosol yields from the photooxidation of 16 different terpenes. *Journal of Geophysical Research*, 111, 1–25.

Lee, S., & Kamens, R.M. (2005). Particle nucleation from the reaction of α-pinene and O₃. *Atmospheric Environment*, 39, 6822–6832.

Massman, W.J. (1998). A review of the molecular diffusivities of H₂O, CO₂, CH₄, CO, O₃, SO₂, NH₃, N₂O, NO, and NO₂ in air, O₂ and N₂ near STP. *Atmospheric Environment*, 32, 1111–1127.

Nolting, F., Behnke, W., & Zetzsch, C. (1988). A smog chamber for studies of the reactions of terpenes and alkanes with ozone and OH. *Journal of Atmospheric Chemistry*, 6, 47–59.

O'Dowd, C.D., Jimenez, J.L., Bahreini, R., Flagan, R.C., Seinfeld, J.H., Hämeri, K., Pirjola, L., Kulmala, M., Jennings, S.G., & Hoffmann, T. (2002a). Marine aerosol formation from biogenic iodine emissions. *Nature*, *417*, 632–636.

O'Dowd, C.D., Aalto, P., Hämeri, K., Kulmala, M., & Hoffmann, T. (2002b). Atmospheric particles from organic vapours. *Nature*, *416*, 497–498.

Pathak, R.K., Presto, A.A., Lane, T.E., Stanier, C.O., Donahue, N.M., & Pandis, S.N. (2007). Ozonolysis of α-pinene: parameterization of secondary organic aerosol mass fraction. *Atmospheric Chemistry and Physics*, *7*, 3811–3821.

Paulson, S.E., Chung, M.Y., & Hasson, A.S. (1999). OH radical formation from the gas-phase reaction of ozone with terminal alkenes and the relationship between structure and mechanism. *Journal of Physical Chemistry A*, *103*, 8125–8138.

Presto, A.A., Huff Hartz, K.E., & Donahue, N.M. (2005a). Secondary organic aerosol production from terpene ozonolysis. 2. Effect of NO_X concentration. *Environmental Science and Technology*, *39*, 7046–7054.

Presto, A.A., Huff Hartz, K.E., & Donahue, N.M. (2005b). Secondary organic aerosol production from terpene ozonolysis—1. Effect of UV radiation. *Environmental Science and Technology*, *39*, 7036–7045.

Ripperton, L.A., Jeffries, H.E., & White, O. (1972). Formation of aerosols by reaction of ozone with selected hydrocarbons. *Advances in Chemistry Series*, *113*, 219–231.

Seinfeld, J.H., & Pandis, S.N. (1998). *Atmospheric chemistry and physics*. From Air Pollution to Climate Change, John Wiley: New York.

Shu, Y., & Atkinson, R. (1994). Rate constants for the gas-phase reactions of O_3 with a series of terpenes and OH radical formation from the O_3 reactions with sesquiterpenes at 296 ± 2 K. *International Journal of Chemical Kinetics*, *26*, 1193–1205.

Slowik, J.G., Stroud, C., Bottenheim, J.W., Brickell, P.C., Chang, R.Y.W., Liggio, J., Makar, P.A., Martin, R.V., Moran, M.D., Shantz, N.C., Sjostedt, S.J., van Donkelaar, A., Vlasenko, A., Wiebe, H.A., Xia, A.G., Zhang, J., Leaitch, W.R., & Abbatt, J.P.D. (2010). Characterization of a large biogenic secondary organic aerosol event from eastern Canadian forests. *Atmospheric Chemistry and Physics*, *10*, 2825–2845.

Tillmann, R., Saathoff, H., Brauers, T., Kiendler-Scharr, A., & Mentel, T.F. (2009). Temperature dependence of the rate coefficient for the α-pinene reaction with ozone in the range between 243 K and 303 K. *Physical Chemistry Chemical Physics*, *11*, 2323–2328.

Volkamer, R., Jimenez, J.L., San Martini, F., Dzepina, K., Zhang, Q., Salcedo, D., Molina, L.T., Worsnop, D.R., & Molina, M.J. (2006). Secondary organic aerosol formation from anthropogenic air pollution: rapid and higher than expected. *Geophysical Research. Letters*, *33*, L17811.

von Hessberg, C., von Hessberg, P., Pöschl, U., Bilde, M., Nielsen, O.J., & Moortgat, G.K. (2009). Temperature and humidity dependence of secondary organic aerosol yield from the ozonolysis of β-pinene. *Atmospheric Chemistry and Physics*, *9*, 3583–3599.

Witter, M., Berndt, T., Böge, O., Stratmann, F., & Heintzenberg, J. (2002). Gas-phase ozonolysis: rate coefficients for a series of terpenes and rate coefficients and OH yields for 2-methyl-2-butene and 2,3-dimethyl-2-butene. *International Journal of Chemical Kinetics*, *34*, 394–403.

Wolf, L., Suhm, M.A., & Zeuch, T. (2009). Suppressed particle formation by kinetically controlled ozone removal: revealing the role of transient-species chemistry during alkene ozonolysis. *Angewandte Chemie*, *48*, 2231–2235.

Zhang, J., Wilson, W.E., & Lioy, P.J. (1994). Indoor air chemistry: formation of organic acids and aldehydes. *Environmental Science and Technology*, *28*, 1975–1982.

Zhang, Q., Jimenez, J.L., Canagaratna, M.R., Allan, J.D., Coe, H., Ulbrich, I., Alfarra, M.R., Takami, A., Middlebrook, A.M., Sun, Y.L., Dzepina, K., Dunlea, E., Docherty, K., DeCarlo, P.F., Salcedo, D., Onasch, T., Jayne, J.T., Miyoshi, T., Shimono, A., Hatakeyama, S., Takegawa, N., Kondo, Y., Schneider, J., Drewnick, F., Borrmann, S., Weimer, S., Demerjian, K., Williams, P., Bower, K., Bahreini, R., Cottrell, L., Griffin, R.J., Rautiainen, J., Sun, J.Y., Zhang, Y.M., & Worsnop, D.R. (2007). Ubiquity and dominance of oxygenated species in organic aerosols in anthropogenically-influenced Northern Hemisphere midlatitudes. *Geophysical Research Letters*, *34*, L13801.